HIGH-LATITUDE ELECTRODYNAMICS FROM A MULTI-ARRAY NONLINEAR GEOMAGNETIC MODEL

D. Vassiliadis[1], A. J. Klimas[2], B.-H. Ahn[3], R. J. Parks[4], A. Viljanen[5], K. Yumoto[6]

[1] *Universities Space Research Association, NASA/Goddard Space Flight Center, Greenbelt, MD 20771, USA*
[2] *NASA/Goddard Space Flight Center, Code 692, Greenbelt, MD 20771, USA*
[3] *Kyungpook National University, Teachers College, Dept. of Earth Sciences, Taegu, 702-701, Korea*
[4] *Department of Physics, University of Florida, Gainesville, FL 32611, USA*
[5] *Finnish Meteorological Institute, POB 503, Helsinki, FIN 00101, Finland*
[6] *Kyushu University, Dept. Earth & Planet Sci., 33, 6-10-1 Hakozaki Higashiku, Fukuoka, 812-81, Japan*

ABSTRACT

We present a model for the high-latitude geomagnetic disturbances with the goal of studying the time-dependent solar wind-magnetosphere-ionosphere coupling. This nonlinear dynamical model, very different from earlier linear approaches, is based on observations from the WIND and ACE solar wind monitors and the IMAGE and MM210 ground magnetometer arrays. The model performance is evaluated in several activity intervals and shows that the overall amplitude of the disturbance is predicted moderately well. The electrojets and other large-scale spatial structures, however, are not reproduced at a satisfactory level at present, so higher-order terms need to be calculated with an expanded database. A coupling of the model to the KRM electrodynamic model and the Ahn *et al.* [1998] conductance forms the basis of a prediction system for the high-latitude ionospheric circuit.

INTRODUCTION

The geomagnetic state at high latitudes is determined by magnetospheric currents as well as their ionospheric closure [Kelley, 1989] and therefore it is a direct diagnostic of the outer magnetosphere [Nishida, 1978]. Therefore measurement of the surface magnetic field state is important for a number of physical issues including the energy transfer from the solar wind to the magnetosphere and the related question of geoeffectiveness of solar wind structures; the time scales and other dynamical development of the geospace response to solar wind changes; the ionospheric morphology of the global substorm and convection cycles; the propagation and dynamics of traveling convection vortices and other regional and transient structures; etc. Here we model the geomagnetic state in order to follow the magnetospheric dynamics as modulated by the solar wind and estimate the ionospheric energy dissipation following that dynamics. Towards the end of the paper we describe how this geomagnetic model is used as the basis for an electrodynamic modeling of the ionosphere at high latitudes.

Earlier attempts to determine the geomagnetic state have been primarily linear and statistical in nature. Friis-Christensen *et al.* [1985], for example, showed that by classifying the geomagnetic response by the clock angle of the interplanetary magnetic field (IMF), one can recover the patterns of equivalent currents and ultimately relate the activity to the flux transfer cycle and the plasma motion across the geomagnetic field. A similar approach was used in the IZMEM model where the linear response of a large number of mostly high-latitude magnetometers to a standard solar wind key parameter input was computed [Levitin *et al*., 1981; Papitashvili *et al*., 1994]. A different line of work has been to first obtain the electric potential distribution from in-situ measurements [e.g., Heppner and Maynard, 1987; Weimer, 1996] from which the large-scale plasma velocity is obtained as tangent to the equipotential lines. Then the magnetic field distribution on the ground is calculated indirectly applying a Biot-Savart law to ionospheric currents and assuming a distant closure profile for the field-aligned currents. Instead here

we develop an extension of a nonlinear dynamical approach which has given predictive models for magnetic indices [e.g. Vassiliadis *et al*., 1995; 1996].

In the sections below we first describe the overall approach and specific model based on the multi-array data; then evaluate the prediction performance of the model in terms of auroral magnetic indices as well as local measurements. Finally we briefly describe the electrodynamic part of the model which allows further modeling of the large-scale distribution of electric fields and currents.

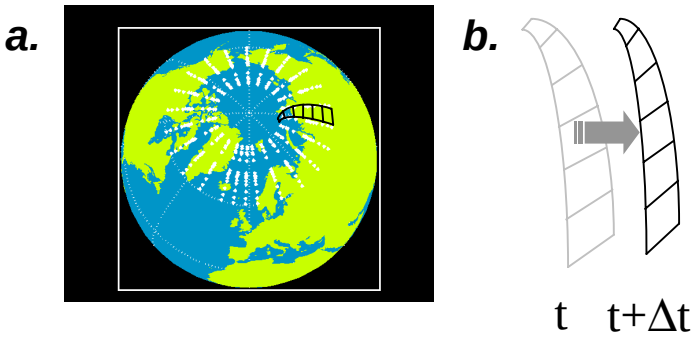

Fig. 1. a. The geographic distribution of IMAGE magnetometers produces a set of "virtual" stations over an annulus at 60-80º. The state variable of the nonlinear model is the vector $\mathbf{B}_x(\lambda,\theta)$ of the North-South component over all latitudes at a local time zone (shown schematically with a narrow grid). b. The time development of the state is given in Eq. (1).

DATA AND METHODOLOGY

In developing the model we have made use of several different magnetometer networks, but here we will discuss results based on only two of them: IMAGE, extending primarily along the Svalbard-Helsinki axis in Fennoscandia, and made available by the Finnish Meteorological Institute; and 5 auroral-zone Siberian and Japanese stations of MM210, an extended network in East Asia, made available by Kyushu University. The latitudinal range of the main array, IMAGE, is approximately 60-80°. The database contains the horizontal field recorded at those stations during January and February of 1995 (although it has been extended significantly at the time this paper was written). These data are binned by local time (as well as by activity later on). In that way we have a coverage of 24x(15+5)=480 "virtual" stations. This provides a more dense grid than obtained from previous modeling or assimilation methods.

Combining data from multiple arrays is useful in several ways: first, during model validation data from one array can be used for training and from the other for testing. Second, combining simultaneous data from several arrays (as well as geomagnetic indices and the recent solar wind key parameters) describes the geomagnetic state in much more detail. IMAGE and MM210 are about 130° apart in longitude so they can constrain the geomagnetic state better. Finally, this results in more accurate modeling in terms of dayside and nightside processes. In combining the two arrays in the way describe below, it is important that the disturbances are scaled correctly: we calculate the quiet-day baseline for each array in a given month from the 5 quietest days.

We develop the field model in a nonlinear analysis approach: the geomagnetic activity is described with a state vector whose dynamics are based on empirical models of the observed activity (in the section on electrodynamics below we supplement this geomagnetic part of the model by several physics-based relations). The state vector contains the horizontal field measured at each station in a fixed local time (Figure 1). Twenty-four of these state vectors, defined at the appropriate equidistant local times, determine the geomagnetic state in an annulus of 60-80° latitude at a resolution of 15° in local time. The time evolution of the state vector at a fixed longitude is determined by its response to either a geomagnetic index or a solar wind input, the latter constructed from the WIND or ACE key parameters. The index input is useful for retrospective studies or, in the future, for nowcasting (when it becomes available in real time), while the solar wind input is being used in forecasting.

The model field $B_x(LT;t)$ for a fixed longitude is then determined by a vector differential equation (the vector containing all IMAGE magnetometers at L as well as the MM210 stations at LT+130°):

$$\frac{dB_x(LT;t)}{dt} = \alpha B_x(LT;t) + \varphi(I(t-T), \frac{dI(t-T)}{dt}, \ldots, \frac{d^{L-1}I(t-T)}{dt^{L-1}}) \qquad (1)$$

A similar equation is used for B_y. The coefficient $1/\alpha$ is a net growth/decay time scale for the ionospheric and field-aligned current systems that determine $\mathbf{B}_x$. The nonlinear function vector ϕ represents the many processes

contributing to the coupling between solar wind and high-latitude magnetospheric-ionospheric activity. The input I(t) is either E_{SW}, where

$$E_{SW} \equiv VB_T \sin^4(\theta/2)$$

$$B_T \equiv \sqrt{B_z^2 + B_y^2}$$

$$\theta = \tan^{-1}(B_z / B_y)$$

or the polar cap index, PC, calculated from the Thule magnetometer in Greenland. The delay T in Eq. (1), representing the earliest electrojet response time, is typically of the order of 20 min, but in all of these runs it has been set to 0. In practice, Eq. (1) is discretized in time and becomes a mapping. An analysis of this type of input-output maps has been given for geomagnetic indices [e.g., Vassiliadis *et al*., 1995; Vassiliadis *et al*., 1996].

It is important to describe how the coefficients of (1) are determined: for the present value of B_x we find all instances in the database when the field vector was similar. Note that the similarity of two state vectors B_x and B_x' is defined simply as the norm of their difference being less than a predetermined constant. The norm is designed to include the recent history of the input. Those state vectors represent times with a similar geomagnetic activity (as well as solar wind activity, if we are using E_{SW} as a driver) as the present one. We fit the subsequent evolution of those similar historical state vectors using Eq. (1) and solve for the coefficients α and ϕ. Then we use those coefficients with the present state vector (and possibly solar wind) to calculate the derivative of the field, again from (1). Clearly the determination of the coupling coefficients from a very small subset of geomagnetic/solar wind conditions (which changes at each time step) produces a very nonlinear model in general. This is called a local-linear model (because of the linearity of Eq. (1).

January 16, 1995, 11:45 UT

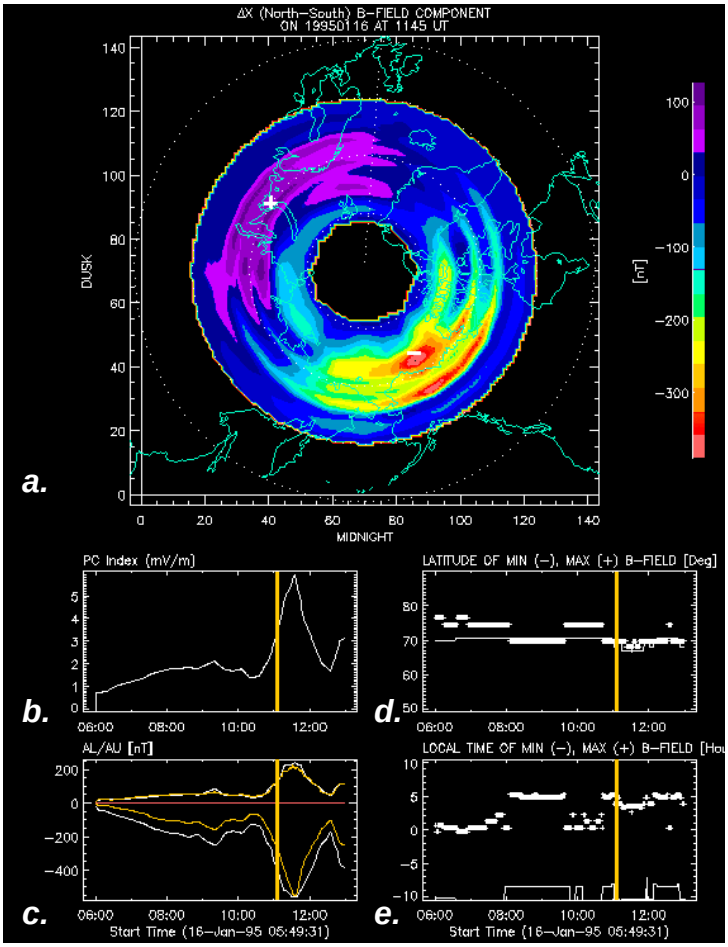

Fig. 2. The graphic output of the geomagnetic model shows the North-South magnetic field component, B_x at high latitudes. Here it is shown during the expansion of the January 16, 1995, substorm. a. A polar view of the B_x component. b. The model input I(t), here the polar cap index, over the course of the substorm. c. We use the minimum and maximum values of B_x to define model "electrojet indices." These are compared with the output of a time series model (red line) [developed by Vassiliadis *et al*., 1996]. d. The latitude of the minimum and maximum $B_x(\lambda,\theta)$. e. The local time of the same extrema. The same type of output plot is made available on-line with the model driven by real-time ACE data (see text).

The field at any position on the annulus can be obtained by interpolating nearby model outputs. Figure 2 shows the output of the model as it is displayed on-line at http://lep694.gsfc.nasa.gov/ RTSM/rt_predictions.html/ except here it is driven by the historical polar cap index rather than the near-real-time ACE solar wind in the website. The minimum and maximum of the field are defined as model "electrojet indices" analogous to AL and AU (Figure 2c). The positions of the extreme values are used as boundary indices (Figure 2d-e) to quantify the displacement of the polar cap and auroral oval.

MODEL RESULTS AND VALIDATION

The model capability in reproducing geomagnetic events is quantified by comparisons against observations. We first compare magnetic indices calculated from the model output and then examine individual magnetometers. The

indices are compared against the Kyoto World Data Center's Quicklook electrojet indices for several levels of geomagnetic disturbance (Note: the Quicklook indices are by definition preliminary and often change as more data become available, so we use them only as a guide). Figure 3 shows the comparison for three recent cases: a northward IMF B_z event (September 15, 1999), a solar wind ejecta event (April 6-7, 2000), and a CME-induced storm (September 22-23, 1999). The 2-hour variations in the first and third event (parts a and c of the figure) are well reproduced. Regrettably any activity with AL<-600 nT is clipped in the nonlinear model, because our database at the time of testing did not contain any events with AL below that level. (Recently higher-activity intervals have been added to the database and a second testing will be conducted.) On the other hand the unusual storm due to ejecta in the solar wind is not predicted well. Only its onset is predicted qualitatively. Overall, however, except for the clipping the agreement between model output and observed preliminary indices is moderately good.

A closer look at the model reveals where the largest uncertainty in model output should be expected and perhaps not surprisingly that region is the central auroral zone (70-73º, between stations BJN and TRO). The average model error is highest in that region. To illustrate that here we examine a moderate substorm that occurred on January 16, 1995 caused by a high-speed stream and lasting ~3.5 hours (Figure 4). Input to the model is provided by key parameters measured by WIND. The model output, the field **B**(LT, θ; t) is calculated from the MM210 stations of the model. That output is evaluated at the locations of the IMAGE magnetometers which are on the dawn side (07:00 LT) at the beginning of the event. The magnetograms are arranged in order of decreasing latitude. The small growth phase and sudden expansion of the poleward magnetometers is reproduced well. In the central part of the auroral zone, however, the activity is predicted with the wrong sign (positive instead of negative) showing that the latitudinal boundary between the eastward and westward electrojets is determined with an error of ~7°. One of us (RJP) has investigated a range of model parameters and found that the prediction error for this substorm does not change significantly. That work has shown the need for a more encompassing database. The recent addition of higher-activity intervals is expected to improve determination of the boundary. Going further south, the last few IMAGE magnetometers are beyond the MM210 range (Figure 4, marked with an 'X"), so the corresponding errors are not evaluated.

NBZ event: September 15, 1999

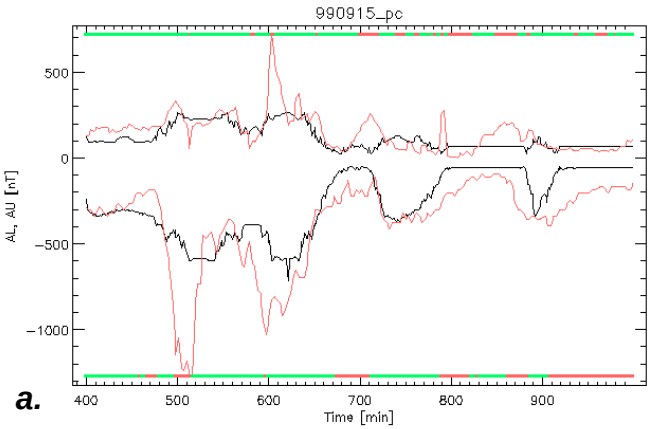

Solar wind ejecta event, April 6-7, 2000

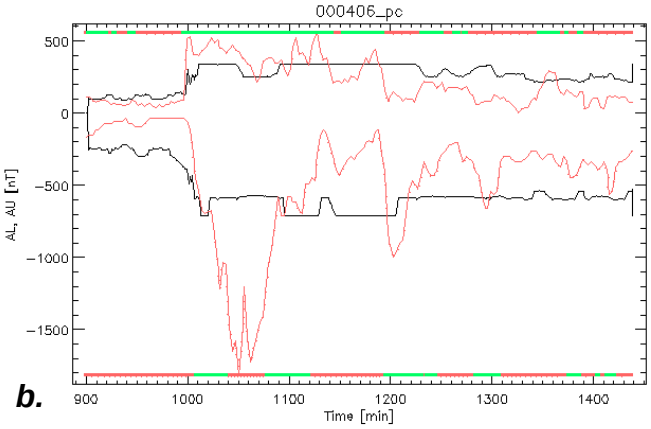

Storm, September 22-23, 1999

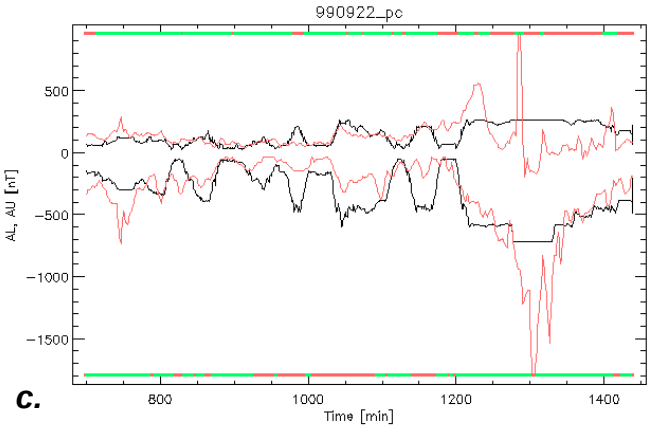

Fig. 3. Comparison of model AL/AU indices with the Quicklook indices of the Kyoto World Data Center: a. A northward IMF B_z interval leads to reverse convection in September 15, 1999. b. A storm produced by solar wind ejecta on April 6-7, 2000. c. A CME-induced storm on September 22-23, 1999. There is fair agreement between predictions and observations for the first and third interval; the second interval is predicted poorly. Note that the artificial "clipping" of high activity is due to lack of many high-activity intervals in the database at this stage.

ELECTRODYNAMIC MODELING

Recently we have extended the model into a simple high-latitude electrodynamic model. From the geomagnetic field distribution $B_x(\lambda,\theta)$ one can obtain the equivalent current function, Ψ. Then using model Hall and Pedersen conductances, σ_H and σ_P, one can solve the two-dimensional Ohm's law for the electric potential distribution $\Phi(\lambda, \theta)$ as originally shown in the KRM method [Kamide *et al*., 1981]:

$$\sigma_H \sin\theta \frac{\partial^2\Phi}{\partial\theta^2} + \left(\frac{\partial(\sigma_H \sin\theta)}{\partial\theta} + \frac{\partial\sigma_P}{\partial\lambda} \right) \frac{\partial\Phi}{\partial\theta} + \frac{\sigma_H}{\sin\theta} \frac{\partial^2\Phi}{\partial\lambda^2} + \left(\frac{\partial\sigma_P}{\partial\theta} - \frac{\partial(\sigma_H / \sin\theta)}{\partial\lambda} \right) \frac{\partial\Phi}{\partial\lambda} = \frac{\partial(\sin\theta \frac{\partial\Psi}{\partial\theta})}{\partial\theta} - \frac{1}{\sin\theta} \frac{\partial^2\Psi}{\partial\lambda^2}$$

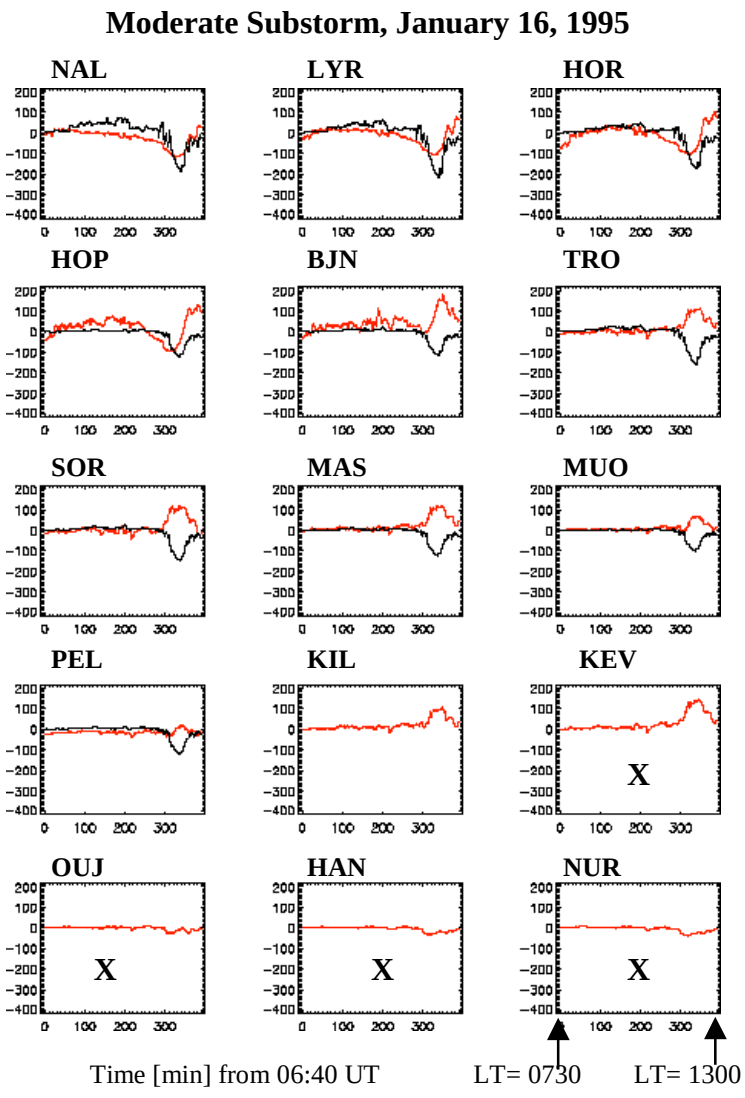

Fig. 4. Comparison of the MM210-based model field with IMAGE observations during the January 16, 1995, substorm. The array is on the dayside during the interval and the 15 magnetograms have been arranged in decreasing latitude. In the last 4 graphs, "X" indicates the locations outside the MM210 latitudinal range. There is good agreement in the poleward edge of the auroral zone and points north, but in the central auroral zone the agreement is poor: the boundary between eastward and westward electrojet is incorrectly determined (error: ~7°). In that region the sign of the modeled disturbance is opposite from observations, although the magnitude is approximately correct.

We use the Ahn *et al.* [1998] model for the Hall and Pedersen height-integrated conductances as functions of the magnitude of the horizontal magnetic field component. The time development of conductances is visually consistent with UV images of the auroral zone (e.g. from Polar) while the electric field is organized is two large-scale cells of unequal size and magnitude as shown by Weimer *et al*. [1996].

CONCLUSIONS AND OUTLOOK

As we are developing a new modeling approach for the high-latitude geomagnetic field we discover its strengths and weaknesses relative to earlier methods. The overall amplitude of the disturbance, as quantified by electrojet indices, is predicted moderately well. Also the spatial pattern agrees with substorm phenomenology. The spatial pattern of the disturbance, however, shows some significant deficiencies. These concern the placement of boundaries, such as the intra-electrojet boundary and also, although less discussed, the equatorward extent of the auroral zone. Clearly significantly more measurements need to be added to the database. We have extended the database by 100% at the time of writing and plan to continue adding more observations. In addition, we have identified 5 intervals of characteristic activity ranging from Northward B_z to a strong storm (3 of them are shown in Figure 3) to test the solar wind geoeffectiveness.

The electrodynamic part of the model is currently undergoing several changes both in the form of the equations as well as the conductance, especially to represent rapidly changing conditions such as occur in substorm expansion. Nevertheless these early results indicate that the amplitude as well as the spatial pattern of geomagnetic activity may be eventually predictable.

ACKNOWLEDGMENTS

We thank NASA/GSFC/CDAWeb for providing archive data for WIND and NOAA/SEC for providing real-time ACE data. As mentioned above the model was originally set up for real-time operation in the SCOSTEP S-RAMP campaign and ISR World Days intervals in September 1999.

REFERENCES

Ahn, B.-H., A. D. Richmond, H. W. Kroehl, B. A. Emery, O. de la Beaujardiere, and S.-I. Akasofu, An ionospheric conductance model based on ground magnetic disturbance data, *J. Geophys. Res.* 103, A7, 14,769-14,780, 1998.

Friis-Christensen, E., Y. Kamide, A. D. Richmond, and S. Matsushita, Interplanetary magnetic field control of high-latitude electric fields and currents determined from Greenland magnetometer data, *J. Geophys. Res.* 90, A2, 1325-1338, 1985.

Heppner, J.P., and N. C. Maynard, Empirical high-latitude electric field models, *J. Geophys. Res.* 92, A5, 4467-4489, 1987.

Levitin, A.E., R. G. Afonina, B.A. Belov, Y.I. Feldstein, Geomagnetic-variation and field-aligned currents at northern high-latitudes, and their relations to the solar wind parameters, *Phil. Trans. Roy. Soc. A*, 304, 1484, 253-301, 1982.

Kamide, Y., A. D. Richmond, and S. Matsushita, Estimation of ionospheric electric fields, ionospheric currents and field-aligned currents from ground magnetometer records, *J. Geophys. Res.* 86, A2, 801-813, 1981.

Kelley, M.C., *The Earth's ionosphere: plasma physics and electrodynamics*, Academic Press, San Diego, 1989.

Nishida, A., *Geomagnetic diagnosis of the magnetosphere*, Springer Verlag, New York, 1978.

Papitashvili, V.O., B. A. Belov, D. S. Faermark, Ya. I. Feldstein, S. A. Golyshev, L. I. Gromova, and A. E. Levitin, Electric potential patterns in the northern and southern polar regions parameterized by the interplanetary magnetic field, *J. Geophys. Res*. 99, A7, 13,251-13,262, 1994.

Vassiliadis, D., A. J. Klimas, D. N. Baker and D. A. Roberts, A description of solar wind-magnetosphere coupling based on nonlinear filters, *J. Geophys. Res.* 100, A3, 3495-3512, 1995.

Vassiliadis, D., V. Angelopoulos, D. N. Baker, and A. J. Klimas, The relation between northern polar cap and auroral electrojet geomagnetic indices in the wintertime, *Geophys. Res. Lett.* 23, 20, 2,781-2,784, 1996.

Weimer, D.R., A flexible, IMF-dependent model of high-latitude electric potentials having 'space weather' applications, *Geophys. Res. Lett.* 23, 18, 2549-2552, 1996.